Reduction of Torque Ripple in Synchronous Reluctance Machines through Flux Barrier Shift

Reduction of Torque Ripple in Synchronous Reluctance Machines through Flux Barrier Shift

Simone Ferrari, *Student Member, IEEE*, Gianmario Pellegrino, *Senior Member, IEEE*,
Matteo Davoli and Claudio Bianchini

***Abstract*—Synchronous Reluctance (SyR) machines are a viable alternative to other kinds of electrical machines in many fields. The simple rotor structure allows a high efficiency level with low manufacturing costs and higher safety in high-speed operations. However, one of the main problems of the SyR machines is the torque ripple generated by the interaction of the stator and rotor Magneto-Motive Force harmonics. Many design solutions have been proposed to date, but heavy torque ripple reduction has only been achieved with long optimizations runs or with complex machine structures. This paper presents an easy and effective method to reduce torque ripple through flux barrier shift. Two machines were designed in order to compare the proposed design with a state-of-the-art procedure. The machines designed with flux barrier shift presents similar performances to the optimized machine, with a lower design time and a more general design method.**

***Index Terms*—Electric Motor, Rotating Machines, AC Motor, Synchronous Reluctance Machine, Torque Ripple**

I. Introduction

In recent years, Synchronous Reluctance (SyR) machines have been established as a viable alternative to other kind of electrical machines in many different fields. The main advantages of this technology are the manufacturing easiness and the absence of Permanent Magnets (PMs) and rotor conductor. These features fit with the different requirements in most of the technological areas where electrical machines are used. In industrial applications, SyR machine features means low manufacturing costs and high efficiency, required by new regulations [1]. In transportation electrification, SyR machines guarantee high efficiency, good flux-weakening properties and safe against faults at high speed [2], [3]. On the other side, one of the main drawback of SyR machines is the torque ripple, that can be high if wrong design choices are followed. Torque ripple in this kind of machine is caused by the interaction of stator and rotor high order unwanted harmonics [4]. Many papers deal with the definition of a standard design procedure for low-torque-ripple machines. In [4] the torque ripple problem was formalized, and a general procedure to design symmetric rotor was presented. The high harmonic interaction between stator and rotor were avoided using a proper rotor "slot" number. The designed machines have symmetrical rotor, but the results can be not optimal. A similar approach was followed in [5], where a stator with odd number of slots per pole pairs n_s was coupled with an even number of rotor "slots" per pole pairs n_r. Also following this methodology, the designed machines are symmetrical, but the unconventional stator can be more difficult to manage. Staying on symmetrical machines, a third approach, is the use of optimization tools for the SyR machines design, as [9]. With this method, the obtained solution can be considered as optimal (after some optimization runs), but the generality of the results is lost, and the computational time can be very long. A different approach to the low-torque-ripple SyR machines design is the use of asymmetrical rotors. One of the first attempts in this field was [7], where a 3 pole pairs machine ($p = 3$) was analyzed and different versions (both symmetric and asymmetric) were compared. At the end, the results were good, but no relation with the torque ripple harmonics was found, and no general procedures were suggested. A further improvement in this field was done in [8], where a 2 pole pairs machine with 2 flux barriers was designed using a complete asymmetric structure (i.e. each rotor pole different from the others). Good results were achieved with this work, but also many problems were highlighted, as the necessity to maintain a sort of symmetry in the machine to avoid unbalanced radial forces. Also in this case, no general procedures, suitable for any pole pairs number or any flux barriers number were proposed. A different approach were presented in [6], where a 2 pole pairs low-torque-ripple machine were designed as a fusion of two high-torque-ripple machines. The results were interesting: the designed rotor was characterized by two big poles and two small poles. The pole displacement was studied in order to avoid unbalanced rotor forces by placing the equal poles on the opposite sides of the rotor. By the way, the proposed procedure was based on the torque ripple analysis of a big number of machines, and it is hardly applicable to other geometries. In [10], a general procedure to design asymmetric rotor was introduced and Finite Elements Analysis (FEA) results were presented for three machines (with 2, 3 and 4 pole pairs). The method, called Flux Barrier Shift (FBS), is based on the spatial shift of the d-axes of the machine, with a symmetry on half machine. The shift angle is computed starting from the unwanted torque ripple harmonic that should be deleted. A possible improvement of this technique is on the mean torque: the

S. Ferrari and G. Pellegrino are with the Department of Energy *"Galileo Ferraris"*, Politecnico di Torino, Torino, Italy (e-mails: simone.ferrari@polito.it and gianmario.pellegrino@polito.it).

M. Davoli is with Raw Power s.r.l., Reggio Emilia, Italy (e-mail: matteo.davoli@rawpowergroup.it)

C. Bianchini is with DISMI - Department of Sciences and Methods for Engineering, University of Modena and Reggio Emilia, Reggio Emilia, Italy (e-mail: claudio.bianchini@unimore.it)

change of the span between two consecutive q-axes cause a slightly reduction of the output torque of the shifted machine. This effect takes place only if $p > 2$.

In this paper, the FBS concept is studied and slightly modified, in order to overcome the associated torque reduction and generalize the method to any number of pole pairs. The main contributions are:

- Apply the same FBS shift angle to each pole pair. This approach is independent from the number of poles and tends to overcome the torque reduction;
- Provide a theoretical interpretation of such FBS approach;
- Embed the FBS methodology in a general design procedure;
- Validate the proposed design flowchart against a state-of-the-art design, where torque ripple was minimized through an optimization algorithm.

The proposed FBS procedure is embedded in SyR-e [14], a Matlab-based tool for the design, optimization and FEA evaluation of SyR and SPM machines.

II. Torque Ripple in Synchronous Reluctance Machines

A. Simplified torque ripple model

According to [5] and [11], torque ripple in SyR machines is caused by the interaction of the stator Magneto-Motive Force (MMF) f_s with the rotor MMF f_r at high harmonic orders. Assuming n_s stator slots per pole pair, f_s will contain the fundamental and all the odd harmonics with order $h = i \cdot n_s \pm 1$, where $i = 1, 2, 3, ...$ The even harmonics are not present because of the f_s symmetry along the d- and q-axis. About f_r, it can be obtained by sampling f_s with a pattern equal to the rotor slots distribution. Assuming n_r equally spaced rotor slots per pole pair, f_r will contain the fundamental and all the odd harmonics with order $k = i \cdot n_r \pm h$, with $i = 1, 2, 3, ...$, and h equal to the stator harmonic that created the rotor one. Once the stator and rotor MMF are defined, it is possible to compute the airgap flux density as:

$$B_g = \frac{\mu_0}{g} \cdot (f_s - f_r) \tag{1}$$

where μ_0 is the magnetic permeability of the air and g is the airgap length. The flux density spectrum will contain all the high order harmonics of the two MMF distribution. The B_g harmonic content is increased by two sources: the slot effect and the rotor anisotropy. The slot effect can be modeled as a function defined equal to zero where the stator slots are opened and the rotor ribs are saturated and one elsewhere. The effect on the airgap flux density is to increase the harmonics amplitude related to the stator ($h = i \cdot n_s \pm 1$). The effect of the rotor anisotropy is more difficult to model. It will be shown in the following that the rotor anysotropy, joined to the stator higher harmonic content, induces a variation of the B_g harmonic components depending on the rotor position.

TABLE I
Main data of the benchmark machine

Pole pairs	p	3	-
Number of stator slots per pole pair	n_s	12	-
Stator outer radius	R	87.5	[mm]
Rotor outer radius	r	59.7	[mm]
Airgap length	g	0.33	[mm]
Stack length	l	110	[mm]
Rated current (peak)	i_0	15.15	[A]

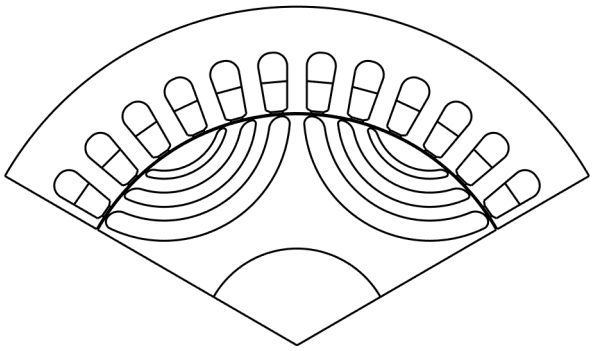

(a)

Fig. 1. Cross-sections of one pole pair of MotA

This fluctuation has a heavy effect on the torque ripple. Torque can be obtained as:

$$T(\theta) = \int_{\xi=0}^{2\pi} B_g(\xi, \theta) \frac{df_s(\xi, \theta)}{d\xi} d\xi \tag{2}$$

It must be remarked that the integral is done on the spatial coordinates, so only the orders contained both in B_g spectrum and in f_s spectrum contribute to machine torque. Torque ripple harmonics is related only to n_s because of f_s spectrum, despite the higher B_g harmonic content. The fluctuation effect introduced by the rotor anisotropy increase the torque ripple, but only if it affects a common order.

B. FEA analysis of a regular machine

The design of regular machines can be based on simple analytical models. According to [11], SyR machines design must be focused on the minimization of the torque ripple and the iron loss. These objectives are pursued by selecting the number of rotor slots starting from the stator slots. The golden rule to correctly relate these two parameters is $n_r = n_s \pm 4$. Table I reports the main data of an induction machine stator [12] that will be used as a benchmark to design and compare different SyR rotor geometries. First, a regular rotor (called MotA) is designed for this stator, following the procedure described in [4]. The number of rotor slots is set equal to $n_r = n_s + 4 = 16$, with three flux barriers per pole, and constant permeance. The final design obtained with the analytical design tool embedded in SyR-e [14] is shown in Fig. 1.

Fig. 2 reports the torque waveform and the related spectrum of MotA, at the rated current in the Maximum Torque Per Ampere (MTPA) condition. The torque ripple harmonics

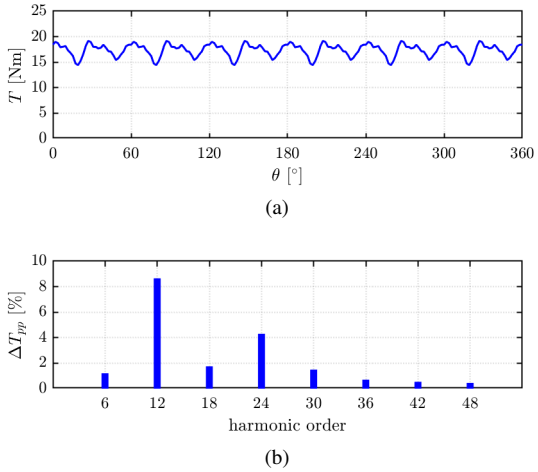

Fig. 2. Rated torque waveform of MotA (a) and torque ripple spectrum (b)

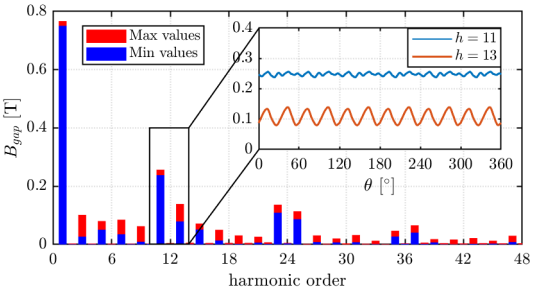

Fig. 3. Spectrum of B_g of MotA for different rotor positions: max values in red and min values in blue. The subplot shows the amplitude of the 11^{th} and 13^{th} harmonic amplitude versus the rotor position

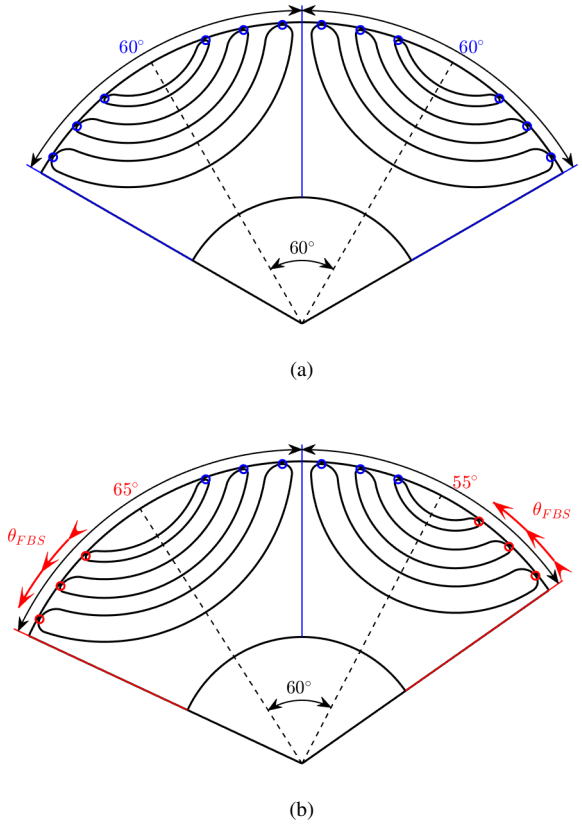

Fig. 4. One pole pair of MotA (a) and MotA-FBS (b). The shifted d-axes of MotA-FBS are highlight in red, and the shift angle is $\theta_{FBS} = 5°$.

are all related to n_s, as explained above. Fig. 3 shows the B_g spectrum for the same working point. The analysis is done for several rotor position, and the variation of the amplitudes is reported in red. In the subplot of Fig. 3, the harmonic orders that produce the main torque ripple component ($h = 12$) are plotted versus the rotor position θ. As addressed above, the oscillations are caused by the interaction of the main stator harmonics and the rotor anisotropy. The main oscillation is for $h = 13$, with 12 periods in $360°elt$.

III. Flux Barrier Shift

A. Shift angle tuning

As explained in the previous section, the variation of B_g spectrum with the rotor position is one of the torque ripple sources. A modification of the rotor anisotropy periodicity can reduce the B_g harmonics fluctuation, reducing the torque ripple. Flux Barrier Shift (FBS) implements this modification by changing the pole pitch of two consequent poles of a well defined angle θ_{FBS}. Fig. 4 shows one rotor pole pair (i.e. one electrical period) of MotA (Fig. 4a) and its shifted version MotA-FBS (Fig. 4b), with $\theta_{FBS} = 5°mech$. The rotor electrical period of MotA-FBS is $120°mech$, and the pitch between the q-axes of the two poles is $60°mech$, as the standard version of the machine (black dashed lines). The d-axes of the shifted machine are reported in blue and red, because they have different properties. The blue d-axis is locked, in the same position of the regular machine, while the red d-axes are moving of θ_{FBS}. This movement cause the pole deformation: one is reduced of the shift angle, and the other is increased of the same quantity. The rotor ribs moves according to their d-axis, as underlined by the color used in the picture.

The tuning of θ_{FBS} can be performed using (3), where θ_{FBS} is expressed in mechanical degree and h is the highest torque harmonic order, equal to the harmonic order of the main oscillation of the B_g amplitudes.

$$\theta_{FBS} = \frac{360}{2\,p\,h} \tag{3}$$

The ribs shift of this quantity leads to a reduction of the h harmonic order, in a similar way as [10]. Starting from a regular machine, the barrier end positions are shifted by the angle θ_{FBS} as show in Fig. 4. Both the regular and shifted rotors can be designed automatically using SyR-e.

B. FEA analysis of a shifted machine

The effect of FBS is noticeable in regular machines. For MotA, the shift angle computed with (3) results in 5 mechanical degree, that correspond to one half of the stator slot pitch. Fig. 5 shows MotA-FBS. From this picture is evident that the alignment with the rotor d-axes and the stator

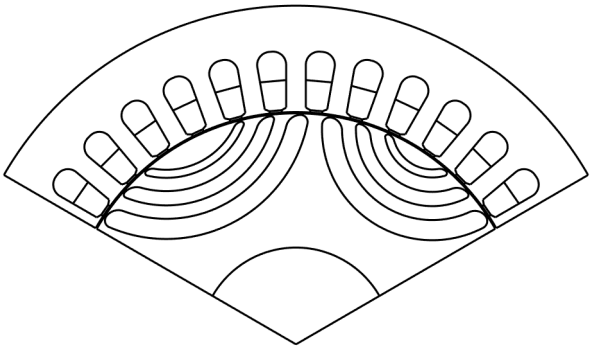

(a)

Fig. 5. Cross-section of one pole pair of MotA-FBS, obtained by the implementation of FBS on MotA.

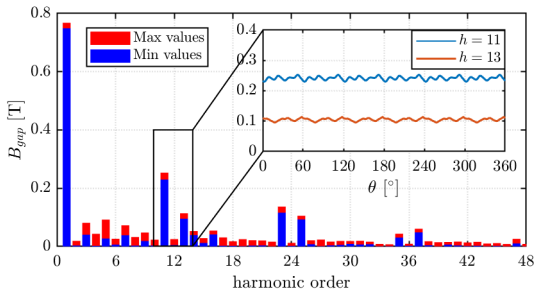

Fig. 6. Spectrum of B_g of MotA-FBS for different rotor positions: maximum values in red and minimum values in blue. The subplot shows the amplitude of the 11^{th} and 13^{th} harmonic versus the rotor position.

teeth is changed from MotA. The extreme d-axes of the figure are aligned with the stator teeth, as for MotA in Fig. 1, while the central d-axis is aligned with the slot. Fig. 6 shows the B_g spectrum of MotA-FBS, in different rotor positions and in the same working point of the analysis of MotA. The shift angle strongly reduces the oscillation of the harmonics with the rotor position, reducing the torque ripple. A side effect is the rise of the even harmonics, due to the asymmetric geometry in the electrical period. Moreover, they does not affect the output torque because they are present only in B_g spectrum and not in f_s spectrum. The torque waveform and spectrum of MotA-FBS are compared with MotA performances in Fig. 7. According to B_g analysis, the 12^{th} torque harmonic is strongly reduced, causing a smoother torque waveform, compared to MotA.

C. FBS-based design procedure

After the FBS definition, it is possible to embed the method in a complete design procedure. The proposed design flowchart is summarized in Fig. 8 and it consist of two steps. First of all, a standard SyR machine must be designed in order to fulfill the specifications of the problem. Good references for this stage are [4], [11] and [14]. Then FBS must be applied to reduce torque ripple. The main torque ripple harmonic can be evaluated with fast FEA simulation or with analytical model. At the end, a FEA validation can

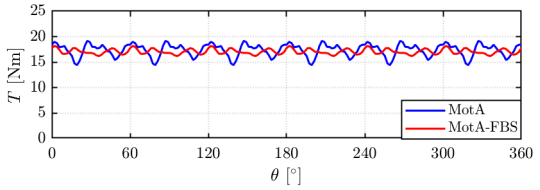

(a)

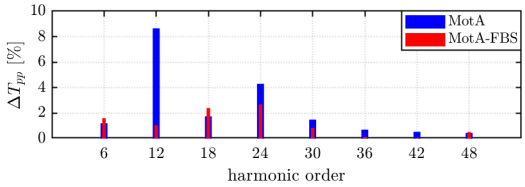

(b)

Fig. 7. Torque waveform (a) and harmonic spectrum (b) of MotA (blue) and MotA-FBS (red) at the rated current, along the MTPA

be performed to verify the effective torque ripple reduction. An example of this design procedure is MotA-FBS. MotA is the results of the first design step, and MotA-FBS is the final design.

IV. FEA Results

In this section, FEA simulations are used to compare the results of the proposed design flowchart and an optimization-based design procedure. The analysis will involve three machines: MotA and MotA-FBS, that represent the first step and the final design of the FBS-based procedure, and MotB [12], that has the same stator of the other machines and the rotor designed using Multi Objective Differential Evolution (MODE) algorithm (embedded in SyR-e). The objectives during the optimization run were maximize the torque and minimize the torque ripple. Fig. 9 shows the cross-section of one pole pair of this machine.

A first comparison between the design procedures can be done on the computational time. The FBS procedure takes few minutes to be completed and most of the time is taken by the FEA simulations used to compute the torque waveform. On the other hand, MODE takes about 6 hours to finish a optimization run, using the parallel computation on four CPU. The computer used for the design processes is a standard workstation with a quad-core CPU Intel Core i7-4770 and 16 GB RAM. Fig. 10 compares the machines performance in therms of mean torque and torque ripple at the rated (1x) and overload (2x) current. MotA and MotA-FBS presents the same mean torque, that is slightly lower than MotB. About torque ripple, MotA is the worst machine, with a torque ripple around 25% at the rated current. MODE reduces torque ripple at circa 18%, but FBS works even better, reducing the torque ripple until 10%. Considering also the heavy differences in the computational time, the powerful of FBS and the proposed design method is evident.

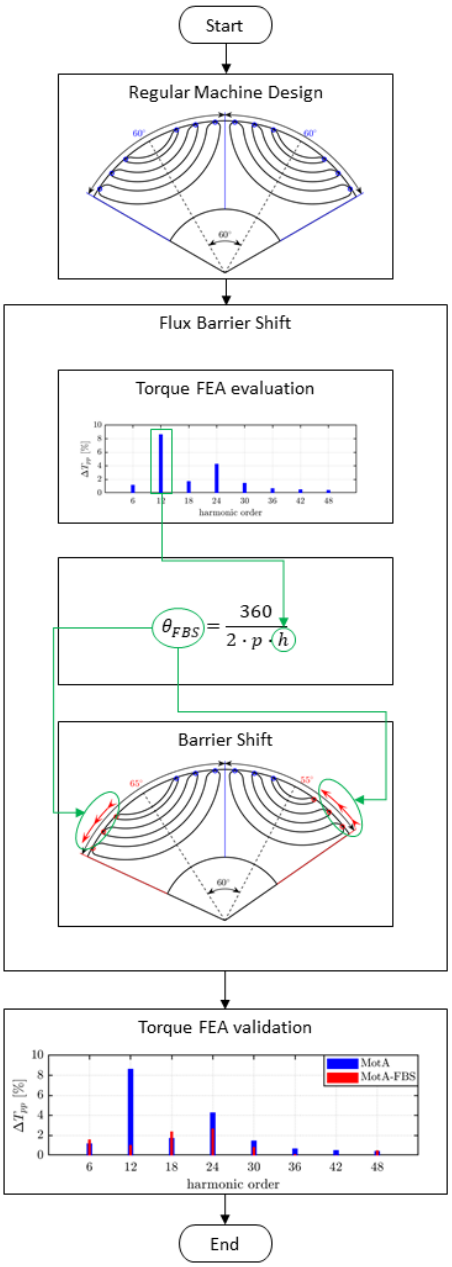

Fig. 8. Flowchart of the proposed FBS-based design procedure

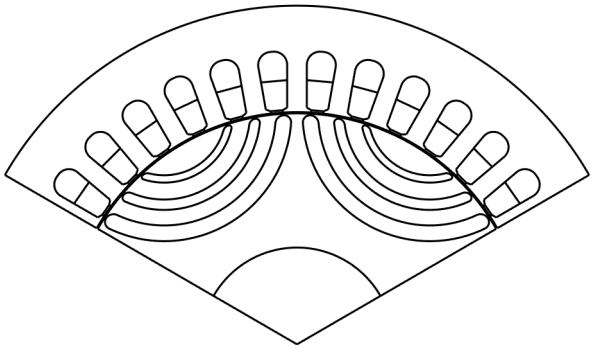

Fig. 9. Cross-section of one pole pair of MotB

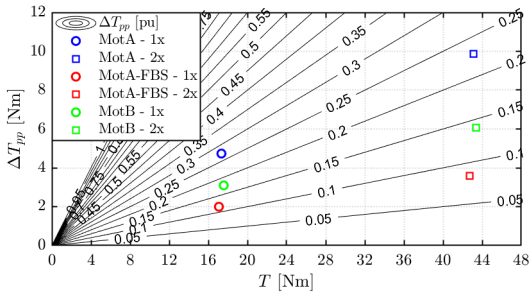

Fig. 10. Torque - torque ripple tradeoff between FBS and optimization algorithm at rated and overload condition

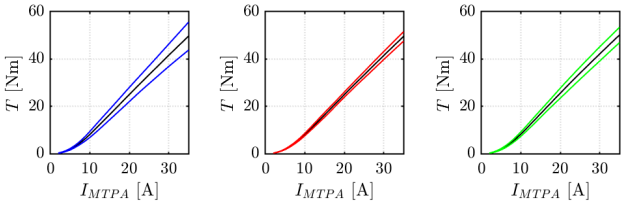

Fig. 11. Torque versus peak current along the MTPA of the three machines involved in the comparison: MotA (a), MotA-FBS (b) and MotB (c). The colored band represent the peak-to-peak torque ripple.

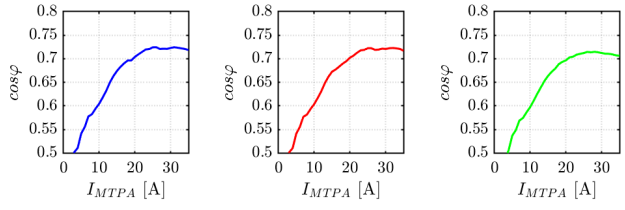

Fig. 12. Power factor versus MTPA current: MotA (a), MotA-FBS (b) and MotB (c)

A. *Torque and Power Factor*

The comparison can be extended on the full operating area. Fig. 11 shows the torques of the three machines versus the current along the MTPA (black lines), with a colored band that represents the peak-to-peak torque ripple. The results obtained for the rated performances holds in all the current range of the machines. The mean output torque of the three motors is similar, the only substantial difference is the torque ripple. Another important performance figure is the power factor $cos\varphi$. Fig. 12 shows the power factor versus the peak current along the MTPA. The three machines presents similar $cos\varphi$ curves, with a little disadvantage of MotB. This analysis tells that FBS doesn't change the magnetic model of the machine, and so, the flux linkages maps.

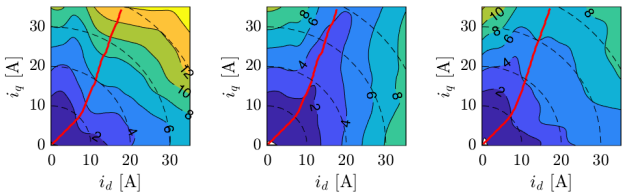

Fig. 13. Absolute value of the peak-to-peak torque ripple contour in the $i_d - i_q$ plane: MotA (a), MotA-FBS (b) and MotB (c). MTPA reported in solid red lines and iso-current contours in dashed black lines

B. Torque ripple map

Flux Barrier Shift deformation affects only the torque ripple, with no penalization of the other performance figures, as pointed out from the previous analysis. To carry out a complete analysis on this feature, the torque ripple is mapped on the full $i_d - i_q$ plane, covering all the possible working points. Fig. 13 shows the torque ripple maps of the three machines involved in the comparison. The MTPA trajectory is reported in red for all the machines, and the current levels are reported in dashed black lines. MotA presents the higher torque ripple, with an evident increase of the amplitude with the mean torque. The shifted machine (MotA-FBS) presents a valley in the torque ripple surface, around the MTPA curve. This shape is due to the harmonic reduction given by FBS: the main ripple harmonic along the MTPA is the same, at all the current level. About MotB, the shape of the torque ripple surface is similar to MotA, but with lower values. The advantage given by FBS is confirmed with this analysis: the torque ripple is reduced in all the practical working point of the machine.

V. Experimental Results

Experimental validation is carried out only on MotB. The validation of MotA and MotA-FBS is ongoing. At this stage, experiments confirm the precision of the software tools used during the design process. Two tests are proposed in the next section: the torque waveform test and the torque ripple map test.

A. Experimental Setup

Fig. 14 shows the test rig for the torque ripple measurement. The prototype is current controlled, and the speed is kept constant by a driving machine and a gearbox. An HBM Gen3i data logger system is used to collect the values measured during the test. They are both electrical (phase current and line voltages) and mechanical (torque and position) quantity. The driving machine and the gearbox permits to keep constant the prototype speed at 10 rpm. This value allows a precise measurement of the torque ripple waveform on one mechanical revolution of the rotor. The gearbox used is a worm gearbox, helpful to avoid the measurement of the driving machine ripple. The low speed also reduces the mechanical filtering effect given by the rotor inertia.

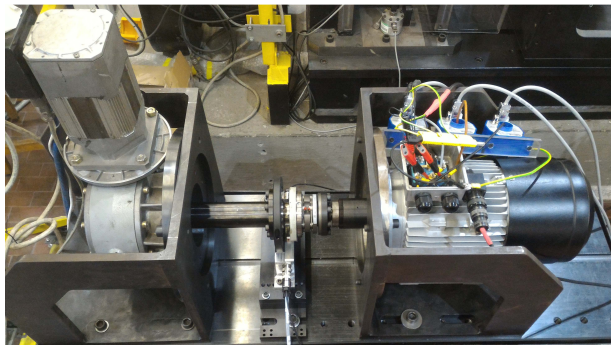

Fig. 14. Test rig for torque ripple measurement: driving machine with worm gearbox on the right and prototype under test on the left.

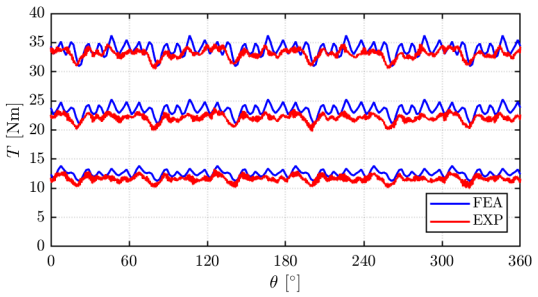

Fig. 15. Comparison between FEA and experimental measurement on the prototype at 12.5, 18.75 and 25 A

B. Torque waveforms

The first test aims to measure the torque waveform versus the rotor position. During this test, the machine is current controlled along the MTPA. Fig. 15 reports the comparison between the torque waveform obtained with FEA and the experimental measurements at 12.5, 18.75 and 25 A (respectively, 80%, 120% and 160% of the thermal rated current). The plot shows a good agreement between FEA and measurements. A small discrepancy in the mean torque exist, and it is related to the end effect, neglected in the FEA. Another difference is the harmonic content: the high frequency ripple is missing in the experimental results. This difference is caused by higher order effect due to the manufacturing process and neglected in the FEA model.

C. Torque ripple map

A more complete test is the torque ripple map. During this experiment, the prototype is current controlled over a regular grid in the dq-plane. Fig. 16 compares the measured peak-to-peak torque ripple map with the FEA results. The MTPA trajectory is reported in solid red line and the current level are plotted in black dashed lines. The match between the two plots is good along the MTPA and for low currents (lower than 20 A). The area with higher discrepancy is for high d-currents and low q-currents, with an underestimation of the torque ripple by the FEA. Furthermore, this points are never used during the normal operation of the machine. As evidenced in the previous test, FEA overestimate the torque

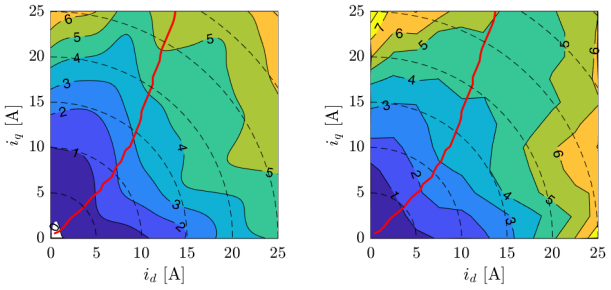

Fig. 16. Peak-to-peak torque ripple map: FEA results (a) and experimental results (b)

ripple at high currents (greater than 20 A). This behavior is due to manufacturing defects, that reduce the high frequency torque ripple harmonics.

VI. Conclusion

An innovative method to reduce torque ripple in SyR machines has been presented. The proposed method deforms the rotor by shifting some rotor flux barriers ends of a well defined angle. The theoretical rules of the torque ripple reduction through FBS has been addressed, and the capability of FBS to reduce the target torque harmonic has been presented both on a test machine. After that, an original and complete design procedure based on regular SyR machines and FBS has been presented and compared with an optimization algorithm. The comparison shows that the two procedures allow to design machines with similar performances, but with different computational time. The FBS-based algorithm allow to design a machine in less than one cent of the time spent by the optimization-based algorithm. Experimental tests are ongoing, and the results on the available prototype validates the FEA simulations and the software tools used during the design process.

References

[1] IEC 60034-30-1 "Rotating electrical machines - Part 30-1: Efficiency classes of line operated AC motors (IE code)".

[2] K. Grace, S. Galioto, K. Bodla and A. El-Refaie, "Carbon-fiber-wrapped synchronous reluctance traction motor," 2017 IEEE Energy Conversion Congress and Exposition (ECCE), Cincinnati, OH, 2017, pp. 3913-3920.

[3] M. Morandin, E. Fornasiero, N. Bianchi and S. Bolognani, "A robust integrated starter/alternator drive adopting a synchronous reluctance machine for automotive applications," 2014 IEEE Transportation Electrification Conference and Expo (ITEC), Dearborn, MI, 2014, pp. 1-6.

[4] A. Vagati, M. Pastorelli, G. Francheschini and S. C. Petrache, "Design of low-torque-ripple synchronous reluctance motors," in IEEE Transactions on Industry Applications, vol. 34, no. 4, pp. 758-765, Jul/Aug 1998.

[5] S. H. Han, T. M. Jahns and W. L. Soong, "Torque Ripple Reduction in Interior Permanent Magnet Synchronous Machines Using the Principle of Mutual Harmonics Exclusion," 2007 IEEE Industry Applications Annual Meeting, New Orleans, LA, 2007, pp. 558-565.

[6] N. Bianchi, S. Bolognani, D. Bon and M. Dai Pre, "Rotor Flux-Barrier Design for Torque Ripple Reduction in Synchronous Reluctance and PM-Assisted Synchronous Reluctance Motors," in IEEE Transactions on Industry Applications, vol. 45, no. 3, pp. 921-928, May-June 2009.

[7] M. Nashiki, A. Satake, Y. Kawai, T. Yokochi and S. Okuma, "A new flux-barrier-type reluctance motor with a slit rotor," in IEEE Transactions on Industrial Electronics, vol. 46, no. 6, pp. 1199-1206, Dec 1999.

[8] M. Sanada, K. Hiramoto, S. Morimoto and Y. Takeda, "Torque ripple improvement for synchronous reluctance motor using an asymmetric flux barrier arrangement," in IEEE Transactions on Industry Applications, vol. 40, no. 4, pp. 1076-1082, July-Aug. 2004.

[9] F. Cupertino, G. Pellegrino and C. Gerada, "Design of Synchronous Reluctance Motors With Multiobjective Optimization Algorithms," in IEEE Transactions on Industry Applications, vol. 50, no. 6, pp. 3617-3627, Nov.-Dec. 2014.

[10] M. Davoli, C. Bianchini, A. Torreggiani and F. Immovilli, "A design method to reduce pulsating torque in PM assisted synchronous reluctance machines with asymmetry of rotor barriers," IECON 2016 - 42nd Annual Conference of the IEEE Industrial Electronics Society, Florence, 2016, pp. 1566-1571.

[11] G. Pellegrino, P. Guglielmi, A. Vagati and F. Villata, "Core Losses and Torque Ripple in IPM Machines: Dedicated Modeling and Design Tradeoff," in IEEE Transactions on Industry Applications, vol. 46, no. 6, pp. 2381-2391, Nov.-Dec. 2010.

[12] C. Bianchini, M. Davoli, G. Pellegrino, F. Immovilli and E. Lorenzani, "Low cost PM synchronous servo-applications employing asynchronous-motor frame," 2015 IEEE Energy Conversion Congress and Exposition (ECCE), Montreal, QC, 2015, pp. 6090-6095.

[13] S. Ferrari, G. Pellegrino, (in press) "FEA-Augmented Design Equations for Synchronous Reluctance Machines," 2018 IEEE Energy Conversion Congress and Exposition (ECCE), Portland, OR, 2018

[14] F. Cupertino et al., "SyR-e: Synchronous Reluctance (machines)-evolution" Internet: https://sourceforge.net/projects/syr-e/. [Mar. 29, 2018]

VII. Biographies

Simone Ferrari received the M. Sc. in Electrical Engineering from Politecnico di Torino, Turin, Italy in 2016, where he is currently working towards his PhD in Electrical Engineering. His PhD research project deals with the development of multi-physical and open-source design tools for electrical machines, especially for synchronous reluctance and PM-assisted synchronous reluctance machines. He is one of the authors of SyR-e, an open-source tool for electrical machines design.

Gianmario Pellegrino, PhD, is an Associate Professor of Electrical Machines and Drives at the Politecnico di Torino, Turin, Italy. Dr. Pellegrino is engaged in several research projects with the industry, and one of the authors of the open-source project SyR-e for the design of electrical motors. He was a visiting fellow at Aalborg University, Denmark, the University of Nottingham, UK, and the University of Wisconsin-Madison, USA. Dr. Pellegrino is an Associate Editor for the IEEE Transactions on Industry Applications and an IEEE Senior Member. He has 36 journal papers, one patent and six Best Paper Awards. He is one of the proponents and members of the PEIC, the Power Electronics Interdepartmental Laboratory established in 2017 at the Politecnico di Torino, a member of the Advisory Board of PCIM Europe. He is currently the Vice President of the CMAEL Association, representing the field of Power Converters, Electrical Machines and Drives in Italy, and the Advisor to the Rector of Politecnico di Torino for the implementation of interdepartmental centers.

Matteo Davoli received the Bachelors and Masters degrees in mechatronic engineering both from the University of Modena and Reggio Emilia, Italy, in 2010 and 2013 respectively. In 2014 he started a Ph.D. school in industrial innovation engineering at the Department of Science and Methods for Engineering at the same University. His research interests include power electronics, electric machines and drives.

Claudio Bianchini, PhD, was born in Italy on September 9, 1974. He received the Dr. Eng. degree in Management Engineering at the University of Modena and Reggio Emilia in 2002, the Dr. Eng. degree in Mechatronic in the 2006 and the Ph.D. in 2010 from the same University. He was an honorary scholar at the University of Wisconsin, Madison, during 2008. His research interests include permanent magnet machines and electric drives. He is the director of the Electric Motor Laboratory at Reggio Emilia Innovazione since 2012.